Available on CMS information server

CMS AN -2010/146

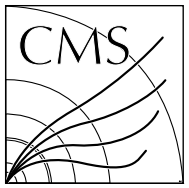

The Compact Muon Solenoid Experiment

Analysis Note

The content of this note is intended for CMS internal use and distribution only

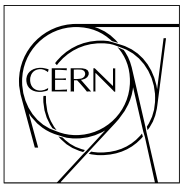

26 May 2010

First Observation Study with Simulated Events of the Decay $B_s \longrightarrow J/\psi\phi$ in pp Collisions at $\sqrt{s} = 7$ TeV

V. Azzolini

University of Helsinki, Finland

G. Cerizza[1)], S. Spanier

University of Tennessee, Knoxville, USA

B. Millan Mejias, A. Schmidt[2)]

University of Zurich, Switzerland

Abstract

We present the analysis of the the decay $B_s \rightarrow J/\psi\phi$, with J/ψ decaying into $\mu^+\mu^-$ and ϕ into K^+K^-. The present note establishes the trigger and reconstruction efficiencies for two selection strategies, one "cut-and-count" signal search and a full maximum likelihood fit with relaxed selection criteria. The final state is reconstructed from a data set of LHC proton-proton collisions at a center-of-mass energy of 7 TeV. The studies presented in this version are purely based on simulated events.

For an integrated luminosity below 1 pb^{-1} we perform the "cut-and-count" analysis in a least biased way by masking a two-dimensional invariant mass region near the expected ϕ and the B_s mean mass positions (blind analysis). In this version of the note we therefore estimate figure-of-merit and the systematic error on our counting result. After unblinding we perform a maximum likelihood fit and treat the analysis as update with increased statistics until the conference.

We extract the final B_S yield for the ICHEP'10 conference with the maximum likelihood fit to the invariant $J/\psi\phi$ mass distribution and the proper decay length distribution. We also attempt to measure the yield as function of the transverse B_s momentum and a value for the proper decay time.

[1)] Contact: gcerizza@utk.edu

[2)] Contact: alexander.schmidt@cern.ch

Contents

1 Introduction

The decay $B_s \to J/\psi\phi \to \mu^+\mu^- K^+K^-$ is of particular interest since it allows the study of many properties of the B_s^0 sytem, such as the differences between the widths and the masses of the two weak eigenstates, B_s^H and B_s^L. The measurement of the interference between mixing and decay might reveal CP violation other than predicted by the Standard Model of Particle Physics indicating the presence of new generations of particles and forces between them [1]. Since $J/\psi\phi$ is a vector-vector final state with an unknown mix of CP-even and CP-odd amplitudes the extraction of CP asymmetries requires an angular analysis [2].

The objective for the Summer'10 conferences is to observe the decay statistically significant and if data permits to extract the B_s lifetime. These measurements do strongly depend on the secondary vertex reconstruction capabilities of the CMS pixel detector and hence serve as benchmark in direct comparison to measurements from the Tevatron [3]. As in the B_d^0 system, the average lifetime of B_S is due to the b quark; it is well measured by the CDF ($\tau = 1.40 \pm 0.14(stat) \pm 0.02(syst) \times 10^{-12}$ s) and D0 experiments ($\tau = 1.444 \pm 0.094(stat) \pm 0.020(syst) \times 10^{-12}$ s) at the Tevatron of Fermilab.

1.1 Strategy

We attempt to measure the cross section for the channel, total and as function of the transverse momentum, and the B_s lifetime. Previous studies [4] indicate that the potential background from prompt J/ψ and inclusive b production can be identified and separated from the signal using the invariant $J/\psi\phi$ mass and the proper decay length ct of reconstructed B_s candidates. We study these and QCD backgrounds with full detector Monte Carlo simulations corresponding to a luminosity at least comparable or exceeding the one expected for real data to develop our strategy. We propose two approaches: one based on optimized selection criteria for event variables ("cut-and-count") and a two-dimensional maximum likelihood fit to the inavriant $J/\psi\phi$ mass and proper decay length ct with relaxed requirements on event variables.

We estimate of the number of $B_s \to J/\psi(\to \mu^+\mu^-)\phi(\to K^+K^-))$ events produced in proton-proton collisions at a center-of-mass (CM) energy of 7 TeV from the cross section for an integrated luminosity of 1 pb^{-1} the following:

$$\begin{aligned}&\sigma(B_s \to J/\psi(\to \mu^+\mu^-)\phi(\to K^+K^-)) = \\ &\quad \sigma(pp \to \bar{b}b) \cdot 2 \cdot B(\bar{b} \to B_s) \cdot \Gamma(B_s \to J/\psi\phi) \cdot \Gamma(J/\psi \to \mu^+\mu^-) \cdot \Gamma(\phi \to K^+K^-)\end{aligned} \quad (1)$$

The value of total cross section for the production of $\bar{b}b$ pairs in proton-proton collisions at a CM energy of 7 TeV is expected to be approximately half of the value at 14 TeV, namely 250 μb [5, 6]. With the branching fractions [3] listed in Table 1.1 we predict that about 2020 events are produced. We establish the efficiency for the trigger and

$B(b \to B_s)$	$(10.7 \pm 1.2)\%$
$\Gamma(B_s \to J/\psi\phi)$	$(1.3 \pm 0.4) \cdot 10^{-3}$
$\Gamma(J/\psi \to \mu^+\mu^-)$	$(5.93 \pm 0.06)\%$
$\Gamma(\phi \to K^+K^-)$	$(48.9 \pm 0.5)\%$

Table 1: *Cross sections and branching fractions from PDG [3].*

the two reconstruction chains in this note. We find the product of both efficiencies to be about 2% which translates into about 40 observed events for each pb^{-1} of integrated luminosity. The luminosity is expected to be known to about 10% which is comparable to the statistical error for the first 3 pb^{-1}. The largest uncertainties in the estimate above of up to 50% are due to the unknown total $pp \to \bar{b}b$ cross section at 7 TeV and the transverse momentum distribution of the b quarks [7].

The blind analysis method has been widely used by the BaBar collaboration and experiments at the Tevatron to establish least biased searches, first or repeated ones [8]. For an integrated luminosity of 1 pb^{-1} we approach a possible signal significance of 5σ, which makes it by definition an observation, a first one at CMS, that corroborates this approach.

1.2 Implementation

We establish here the complete analysis with software releases and simulations available. We expect that the Summer'10 analysis is likely an update with somewhat improved code and newly generated events for signal and background as they become available, but methods are the same and efficiencies will not change by much. The

studies presented here have been performed with analysis software release CMSSW 3.3.6 [9]. Simulations of pp hard scatter use PYTHIA version 6.416 [10]

1.3 To Do

For the Summer'10 analysis the following issues still need to be addressed:

- Reconstruction efficiencies with new software release CMSSW 3.6.x
- QCD background contribution with newly generated samples exceeding the expected luminosity in data
-

2 Simulated Event Samples

Table 2 lists the sets of fully simulated events used in this study. Based on those samples we optimize the event selection and validate the analysis technique. All samples use PYTHIA [10] for simulation of the pp collisions. The signal and the $b\bar{b}$ background are studied in the inclusively generated $b \to J/\psi X$ sample. The EvtGen [11] simulation takes care of all b hadron decays. One of the two b hadrons in the event is forced to decay to a final state with a J/ψ meson, directly or via intermediate excited charmonium states. Events with a J/ψ decaying into two muons are filtered at the generator level by requiring that the two muons have opposite charge and transverse momentum $p_T > 2.5$ GeV/c and a pseudo-rapidity $|\eta| < 2.5$. For detailed studies we also use exclusively generated $B_S \to J/\psi\phi$ and $B_d \to J/\psi K^*$ samples. For the prompt J/ψ background we use a sample of $pp \to J/\psi X$-type events produced with the same generator-level muon filter as the b hadrons samples. For the QCD background we study the inclusive $pp \to \mu\mu X$ sample with the same muon pre- selection requirements on p_T and η as for the other sets above.

In the next iteration we will require that b-hadrons are decayed by EventGen [11].

Process	N_{ev}	σ (pb)	ϵ_{filter} (%)	L (pb^{-1})
$b \to J/\psi X$	5×10^6	66.6×10^6	0.024	31
$pp \to J/\psi X$	10^7	12.6×10^6	0.074	11
$pp \to \mu\mu X$	10^6	48.4	1.12×10^{-5}	1.87

Table 2: For each event sample we list the total number of generated events N_{ev}, the production cross-section σ, the filter efficiency ϵ_{filter}, and the integrated luminosity L. For the $b \to J/\psi X$ sample we derive the integrated luminosity from the $B_s \to J/\psi\phi$ sub-set.

3 Trigger Efficiency Studies

Dependent on the instantaneous luminosity l of LHC different dimuon triggers at Level-1 and at the High Level Trigger (HLT) farm will be implemented by CMS to adjust the data acquisition rate. The first scenario assumes $l_1 \simeq 10^{30}/\text{cm}^2$ s, the second one a factor of 10 higher $l_2 = 10 \cdot l_1$ expected to occur after 10 pb^{-1} of integrated luminosity has been recorded (i.e. likely after ICHEP 2010). For completeness we study preliminary HLT trigger scenarios [12] analoguously to the Level-1 trigger.

We study three different triggers:

- `L1DoubleMuOpen`, a double muon pass-through trigger, where no selection requirements beyond the Level-1 are applied,
- `HLT_doubleMu0`, with at least two muons identified at the Level-3, without any p_T requirement, and
- `HLT_doubleMu3`, with at least two Level-3 muons with $p_T > 2.5$ GeV/c each.

Table 3 summarizes the trigger details.

Trigger	Pre-scale	Rate (Hz)	Signal ϵ %
`L1DoubleMuOpen`	1 (l_1)	5.9	19.3
	50 (l_2)	1.2	
`HLT_doubleMu0`	1 (l_1)	0.4	7.2
	1 (l_2)	3.8	
`HLT_doubleMu3`	1 (l_1)	0.1	4.2
	1 (l_2)	1.2	

Table 3: Trigger scenarios. For each trigger we list the pre-scale factor and the rate for two the instantaneous luminosity scenarios ($l_1 = 10^{30}/\text{cm}^2$ s, $l_2 = 10 \cdot l_1$) and the signal efficiency.

For each trigger scenario we compare the transverse momentum distribution of the two exclusive channels $B_d \to J/\psi K^*$ and $B_s \to J/\psi\phi$ with the original distribution provided by EvtGen [11] (see Figs. 1, 2). The distributions have been normalized to the same area.

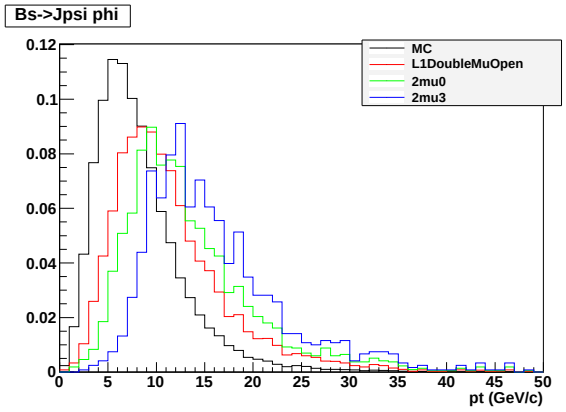

Figure 1: B_s transverse momentum distribution for the generated events and after application of the various triggers.

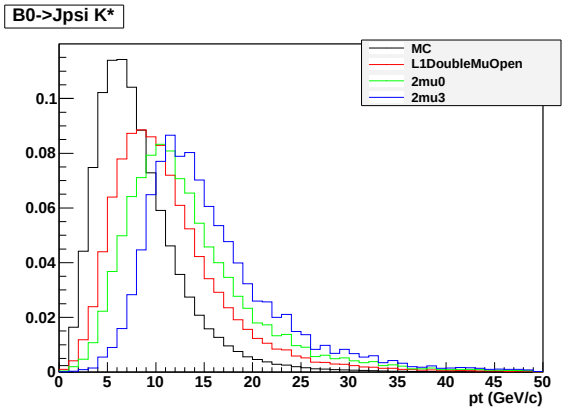

Figure 2: B_d transverse momentum distribution for the generated events and after application of the various triggers.

The p_T dependent efficiency is defined as:

$$\epsilon(p_T^B) = \frac{N_{trg}(p_T^B)}{N_{gen}(p_T^B)} \tag{2}$$

where N_{trig} is the number of events passing the trigger in the given p_T^B bin, and N_{gen} is the number of events generated in the same bin. The trigger efficiencies for all three trigger scenarios as a function of p_T^B are displayed in Fig.3.

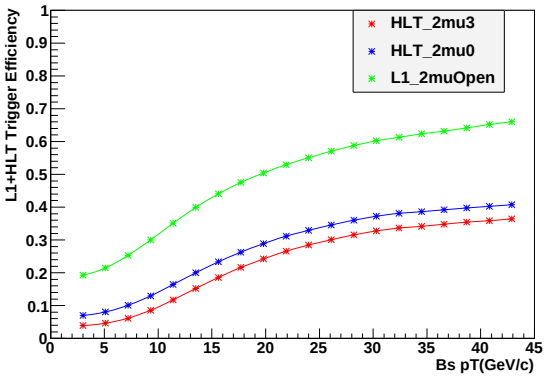

Figure 3: Trigger efficiencies for B_s events for the three trigger scenarios as a function of p_T^B.

Since we use the proper decay length ct as variable to discriminate signal and background, and to measure the proper decay time of the B meson, we study the bias introduced by the different trigger scenarios. Fig. 4 displays the distribution in ct for the different trigger scenarios in a logarithmic event scale. Fig, 5 shows the ratio between the `L1DoubleMuOpen` and the generated events with the statistical error per bin: we observe an insignificant distortion of the original distribution after application of the trigger requirements.

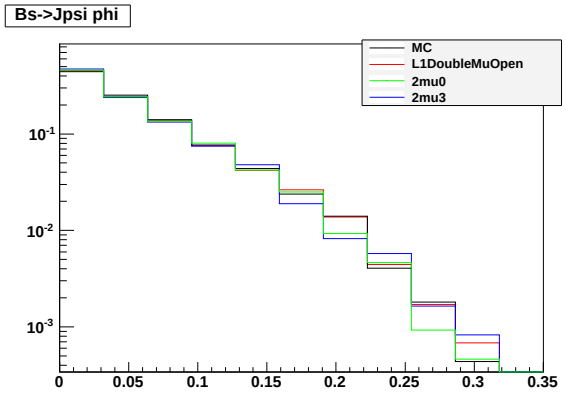

Figure 4: B_s proper decay length distribution for generated events and after application of various trigger scenarios. The colors are explained in the legend.

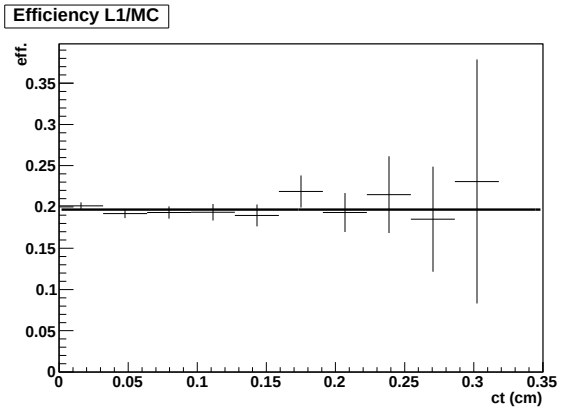

Figure 5: The ratio between signal events passing the L1DoubleMuOpen trigger requirements and generated events. This efficiency is $\epsilon = (19.7 \pm 0.3)\%$.

For completeness we also show the distribution of the total B momentum for the two major B decay channels in Fig. 6, 7.

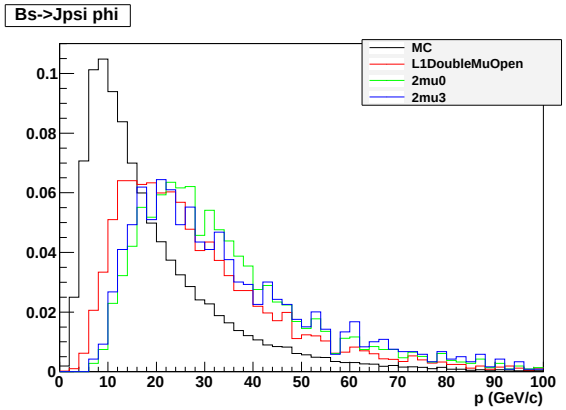

Figure 6: B_s total momentum for simulated $pp \rightarrow B_s \rightarrow J/\psi\phi$ events as generated and after trigger requirements were applied. The colors are explained in the legend.

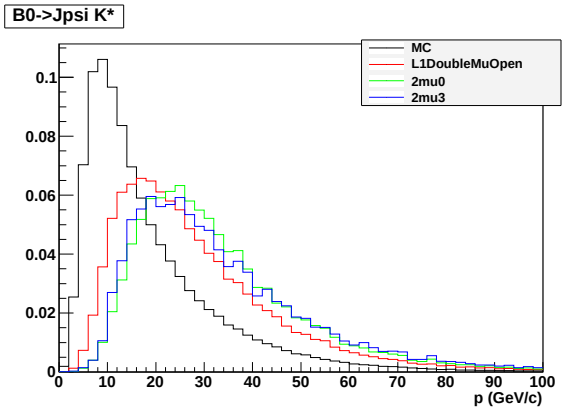

Figure 7: B_d total momentum distribution for simulated $pp \rightarrow B_d \rightarrow J/\psi K^*$ events as generated and after trigger requirements were applied. The colors are explained in the legend.

4 Pre-Selection of B_s Candidates and Kinematic Fit

We start by reconstructing J/ψ candidates from two oppositely charged muons that pass the quality requirements `TM2DCompatibilityTight`[9] and are each associated with a track in the silicon tracker (`GlobalMuon` or `TrackerMuon`). Furthermore, each pair of muons is required to to fulfill energy and momentum conservation . We keep all J/ψ candidates with $p_T > 0.5$ GeV/c and an invariant mass within 150 MeV/c^2 to the world average value [3]. Candidate ϕ mesons are reconstructed from pairs of oppositely charged tracks with $p_T > 0.5$ GeV/c and that are selected from a sample with the above muon candidate tracks removed. We assume each track to be a kaon and calculate the invariant mass of the track pair. We keep combinations with an invariant mass within 50 MeV/c^2 to the world average [3].

We combine a J/ψ and a ϕ candidate to form a B_s candidate and require that the invariant mass lies between 4.5 GeV/c^2 and 6 GeV/c^2. This selection allows us to reduce the number of candidates per event before performing the kinematic fit. The candidates that fulfill all those requirements are then subjected to a kinematic fit [**?**] that requires momentum and energy conservation in the B_s decay and both decay products to originate from a common vertex. It does fit the J/ψ decay and the dimuon pair is constrained to the nominal J/ψ mass value. We select one B_s candidate per event based on the best vertex fit probablility. Furthermore, the fit B_s candidate has to lie within the mass range $5.2 < M_{B_s} < 5.7$ GeV/c^2. This selection identifies the correct $B_s \rightarrow J/\psi\phi$ candidate in 99% of all cases as determined from the associated 'true' signal decay at generator level (Monte Carlo Truth Matching). Fig. 8 shows the invariant $J/\psi\phi$ mass distribution before and after application of the kinematic fit.

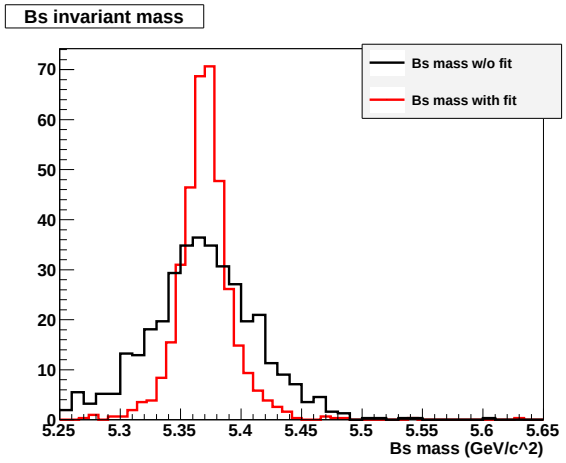

Figure 8: B_s invariant mass before (black) and after (red) the kinematic fit.

We calculate the two-dimensional proper decay length ct for the reconstructed B candidates from the measured distance L_{xy} between the production (or primary) and B-decay vertices projected onto the transverse momentum, and the relativistic boost of the reconstructed B meson in the transverse plane the following:

$$ct = \frac{M_B}{p_T^B} L_{xy} \,, \tag{3}$$

where M_B and p_T^B are the mass and transverse momentum of the B candidate. The transverse flight length L_{xy} is the projection of the vector $\vec{s}$ pointing from the primary to the secondary vertex to the transverse momentum:

$$L_{xy} = \frac{\vec{s} \cdot \vec{p}_T^B}{|\vec{p}_T^B|} \tag{4}$$

The generated value of the mean proper decay length $c\tau = 424$ μm. The single-Gaussian width of the distribution of the difference in ct between reconstructed and generated values as determined by truth-matching for signal events (residual distribution) is approximately 50 μm. The distribution is shown in Fig. 9.

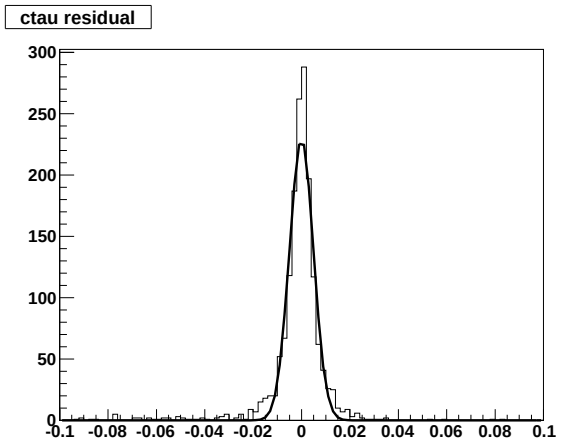

Figure 9: Proper decay length residual distribution in truth-matched signal events.

5 Cut-And-Count Selection of the B_s candidates

For the final analysis we follow two alternative approaches to optimize the signal significance. This choice follows the amount of data available for analysis during the data taking. For the first available data we perform a "cut-and-count" analysis with somewhat tighter requirements on event variables.

5.1 Optimization

We optimize the figure-of-merit in variable space for the counting in a signal area. With N_S the number of signal events, and N_B the number of background events, we define our figure-of-merit, κ, the following:

$$\kappa = \frac{N_S}{\sqrt{N_S + N_B}} \tag{5}$$

which in good approximation estimates the statistical significance for our counting experiment. We distinguish the following categories of potential background:

- Background from other B meson decays.
  An important background results from the decay $B_d \to J/\psi K^*$, with $J/\psi \to \mu^+\mu^-$ and $K^* \to K^+\pi^-$ that has naturally a production rate 7 times larger than our signal and might be mis-identified due to a mis-reconstructed ϕ decay. We use a cocktail of many different B-meson decays to probe for other sources.
- Prompt J/ψ production.
  Since a significant signature of our signal is the J/ψ signal we expect that we are suceptible to production channels where the J/ψ does not originate from a decay of a long-lived particle.
- QCD background.
  Anything that is produced in proton-proton collisions leading to two muons in the final state, but no J/ψ.

The samples are mutually exclusive as verified based on the Monte Carlo truth.

We consider the following event variables:

- the vertex probability from the kinematic fit to the B_s candidate,
- the transverse momentum of both ϕ decay kaon candidates,
- the decay length significance ct/σ_{ct},
- the cosine of the angle α between the direction of flight as reconstructed from the primary and secondary vertices of the B_s candidate and its momentum direction $\cos\alpha$,
- a region in the the K^+K^- invariant mass around the nominal value, and
- a region in the invariant $J/\psi\phi$ mass.

For the latter two we consider a wider range and define subranges for signal and background measurements according to Table 4. The size of the signal box has been chosen to contain 3 standard deviations of the distribution in both variables assuming they distribute according to a single Gaussian - we did not optimize the signal box further, but inspect the figure of merit for our choice. We leave a small gap in the ϕ mass between signal box and side band area to account for the asymmetry in the ϕ distribution that is due to its natural width and its one unit of internal angular momentum. A small gap on the upper side of the B_s mass similarly accounts for an observed minor bleeding of the reconstructed signal. We have verified that these two variables are mostly uncorrelated for the signal due to the impression in the measurement. We find the correlation coefficient to be 9.4%. In the different background components we find to coefficients to be -1.3% in B background, -9.3% in prompt J/ψ, and -2.0% in QCD background.

The distributions in the reconstructed ϕ versus B_s mass plane for the different simulated samples are shown in Fig. 10, the projections are displayed in Fig. 11 and Fig. 12.

Variable	$M(K^+K^-)$ / GeV/c^2	$M(J/\psi\phi$ / GeV/c^2
Full range	0.98 - 1.06	5.25 - 5.65
Signal Box	1.005 - 1.040	5.30 - 5.45
Side Band	0.980 - 1.000 & 1.050 - 1.060	5.25 - 5.30 & 5.47 - 5.65

Table 4: *Definition of regions in reconstructed ϕ and B_s mass for background estimate and signal counting. The signal region will be kept masked until our estimated figure-of-merit exceeds 5.*

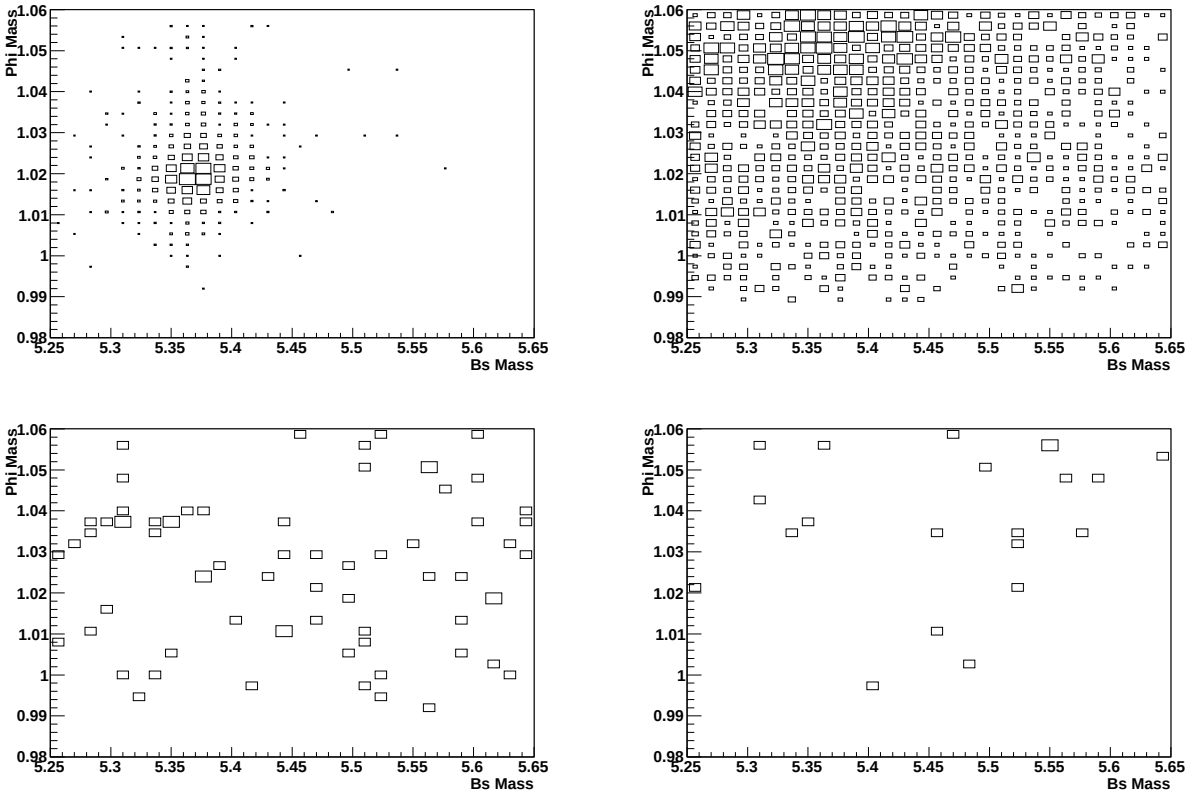

Figure 10: *Reconstructed ϕ versus B_s mass for signal (top left), B background (top right), prompt J/ψ background (bottom left), and $pp \to \mu\mu X$ background (bottom right).*

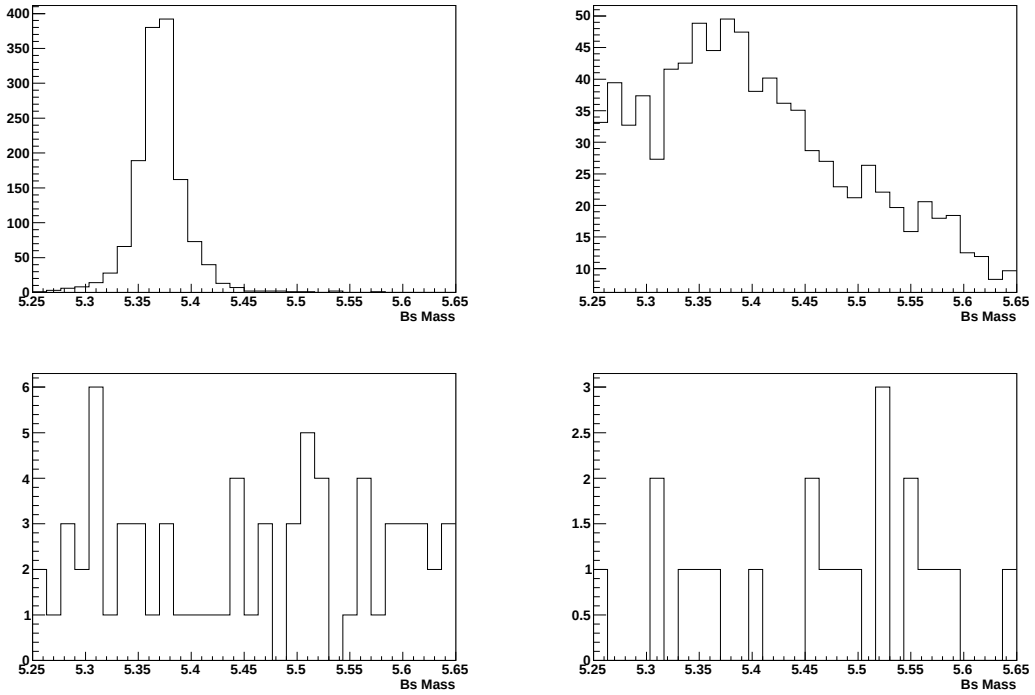

Figure 11: *Reconstructed B_s mass for signal (top left), B background (top right), prompt J/ψ background (bottom left), and $pp \to \mu\mu X$ background (bottom right).*

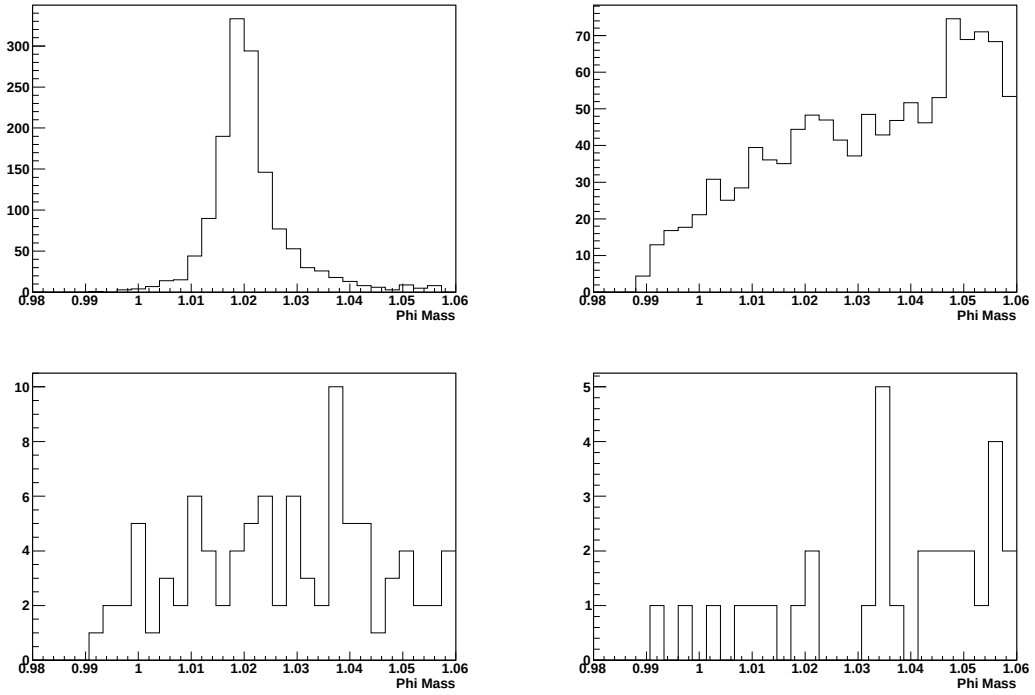

Figure 12: *Reconstructed ϕ mass for signal (top left), B background (top right), prompt J/ψ background (bottom left), and $pp \to \mu\mu X$ background (bottom right).*

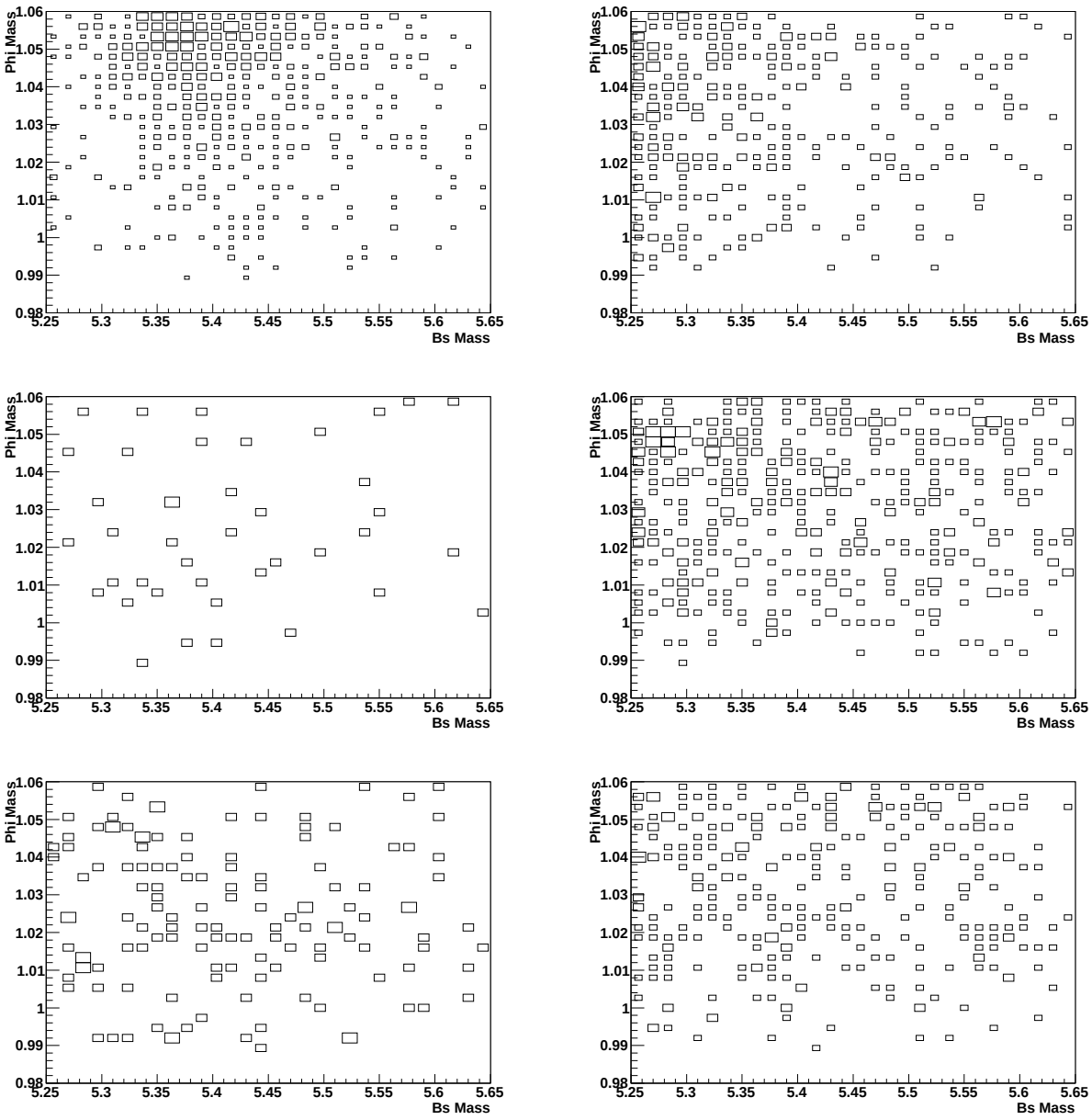

Figure 13: *Reconstructed ϕ versus B_s mass for $J/\psi K^*$ (top left), $J/\psi K_1^0$ (top right), $J/\psi\eta$ (center left), $J/\psi K^+$ (center right), other B_s background (bottom left), and other B_d background (bottom right).*

We decided to apply a cut on the fitted vertex probability at 2% to clean the sample from unlikely misreconstructed background and a minimum cut on the transverse momentum of the kaons at 0.7 GeV/c. Comparing the 2D plot for the signal in Fig. 10 with the different backgrounds in Fig. 13 we decided to cut within 10 MeV around the PDG ϕ mass value to reduce most of the background coming from the $B_d \to J/\psi K^*$ decay.

The Figs. 16 to 18 show the scan of the figure-of-merit in the projections onto the different event variables. Each variable has been plotted applying the cuts on all the other variables. For the final choice of criteria the event reduction is detailed in Table 5. We estimate the figure-of-merit for an integrated luminosity of 1 pb^{-1} to be 5.61.

For a sample of 10 pb^{-1}, we plot the variables M_{B_s} and after the event selection in Fig. 19.

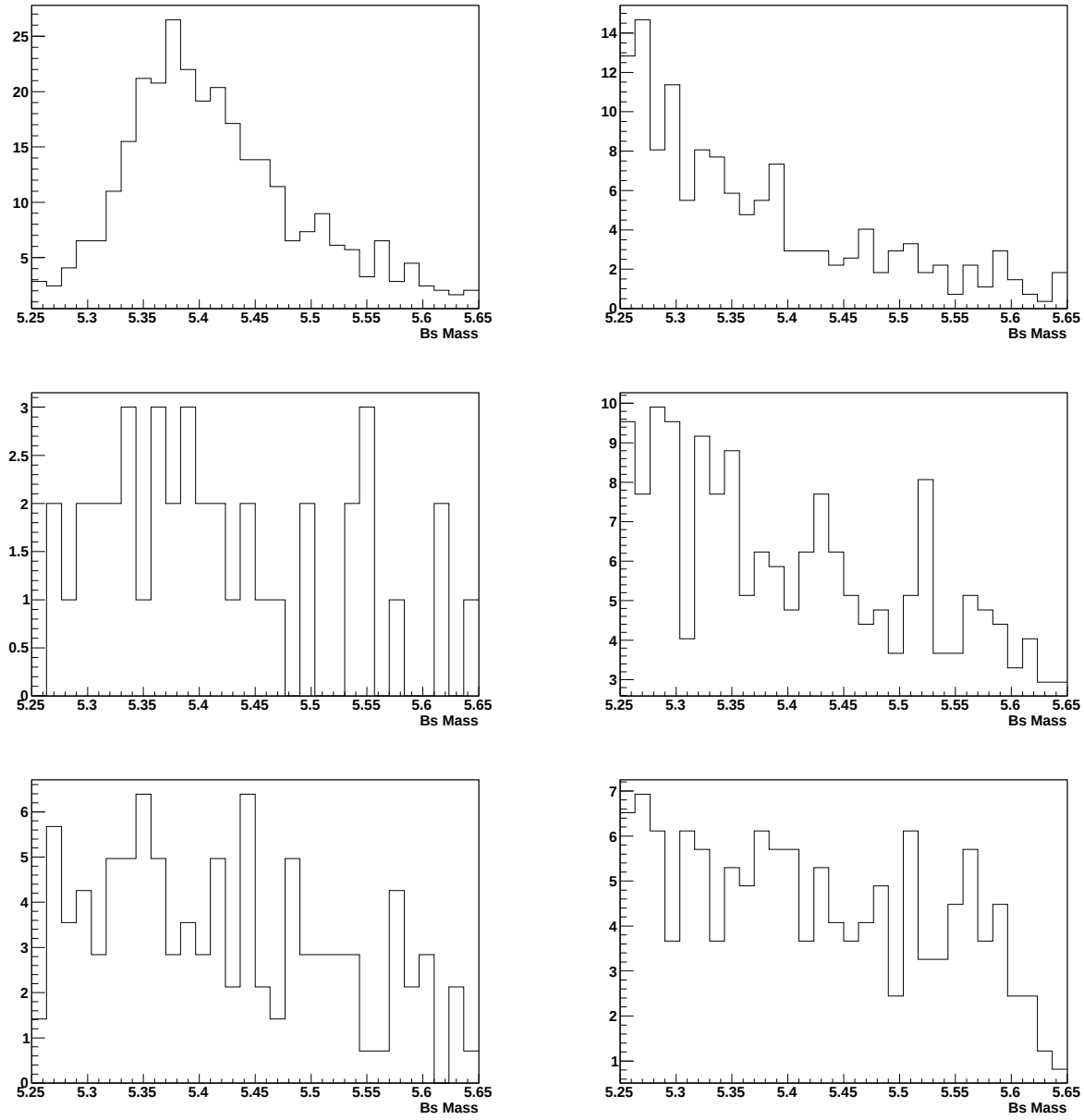

Figure 14: *Reconstructed B_s mass for $J/\psi K^*$ (top left), $J/\psi K_1^0$ (top right), $J/\psi\eta$ (center left), $J/\psi K^+$ (center right), other B_s background (bottom left), and other B_d background (bottom right).*

	$B_s \to J/\psi\phi$	$b \to X$	Prompt J/ψ	$pp \to \mu\mu X$
Number of generated events	970	94736	920247	510216
`L1DoubleMuOpen`	191	17514	98854	210566
Pre Kinem. fit	121	10266	39362	6597
After Kinem. fit	84	1653	3408	1432
Vtx P(KK)>2 %	0.905	0.598	0.706	0.549
Kaon $p_T > 0.7$ GeV/c	0.829	0.395	0.339	0.776
$c\tau/\sigma_{c\tau}$ >3	0.616	0.230	0.090	0.424
$\cos\alpha$ >0.98	0.819	0.318	0.334	0.543
signal box	42	11	1	1
side band	1	26	4	8

Table 5: The table lists the expected number of events in 1 pb^{-1} integrated luminosity for each sample and each optimized cut-and-count selection criterion.

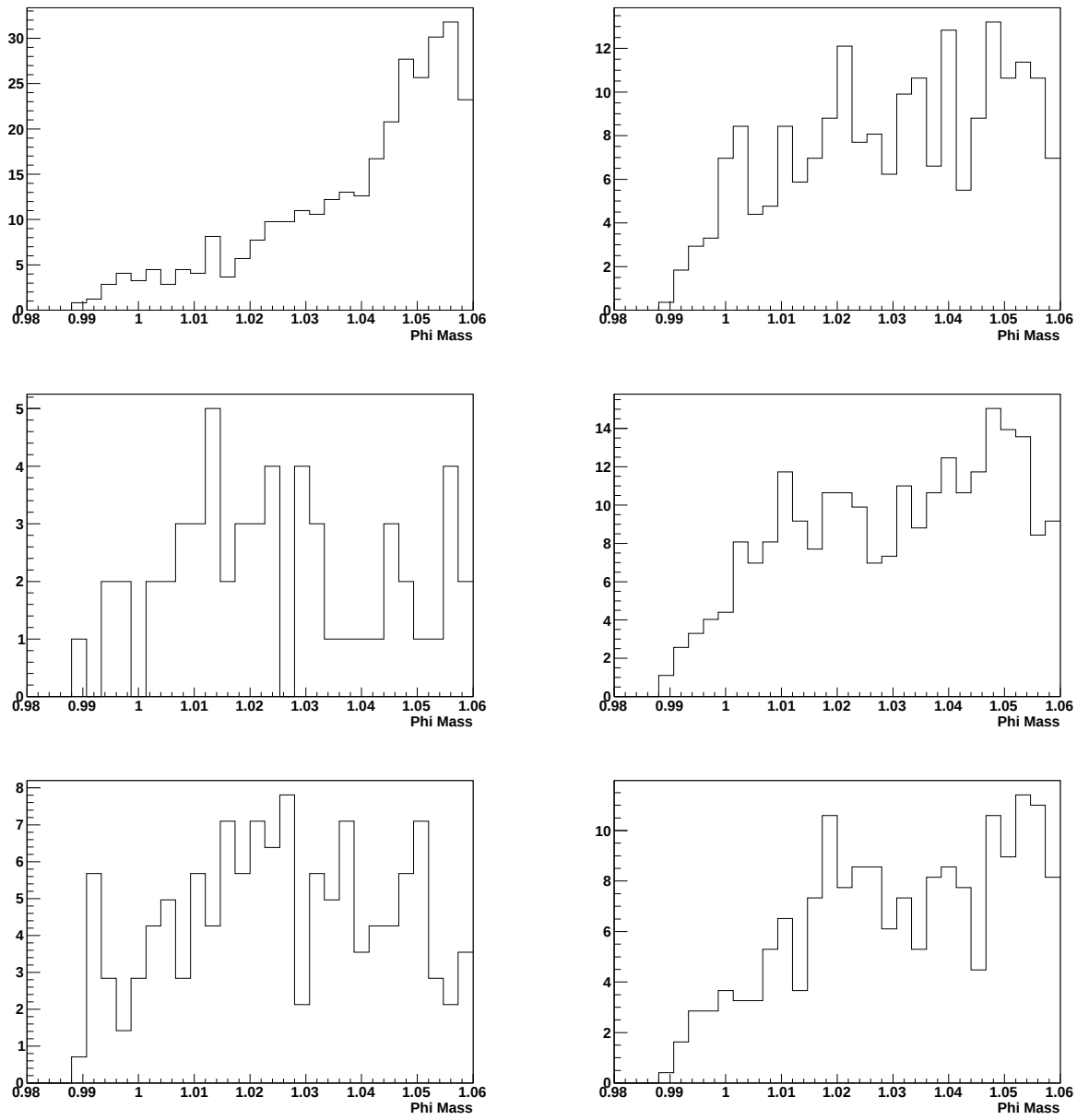

Figure 15: *Reconstructed ϕ mass for $J/\psi K^*$ (top left), $J/\psi K_1^0$ (top right), $J/\psi\eta$ (center left), $J/\psi K^+$ (center right), other B_s background (bottom left), and other B_d background (bottom right).*

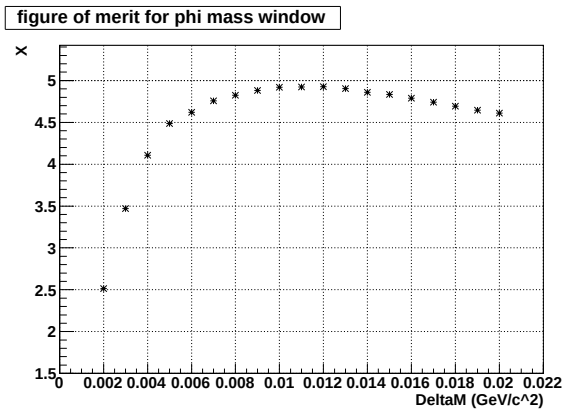

Figure 16: Figure of merit for the ϕ mass window cut.

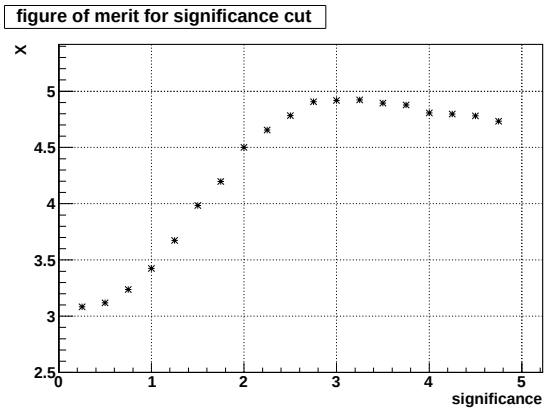

Figure 17: Figure of merit for the $c\tau/\sigma_{c\tau}$ cut.

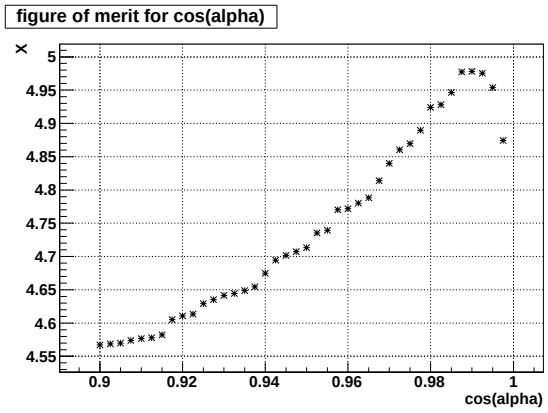

Figure 18: Figure of merit for the $\cos(\alpha)$ cut.

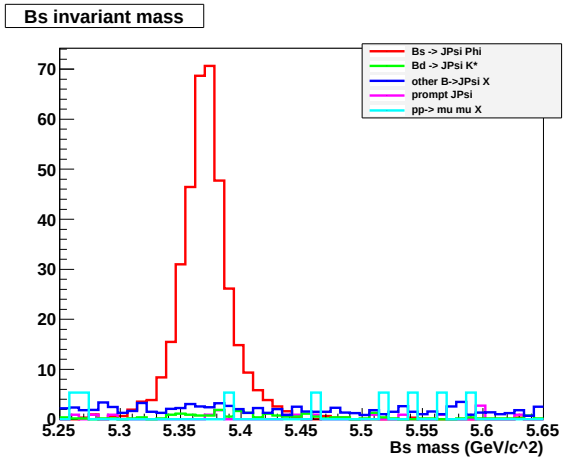

Figure 19: Reconstructed B_s mass distribution after the cut-and-count selection with a relaxed cut on $\cos\alpha > 0.8$ for signal and background categories and an assumed integrated luminosity of 10 pb^{-1}.

5.2 Background Studies from Data

An additional step is the establishment of the background from real data. We will measure the variation of the background level in the side band as function of the event variable criteria with the masked signal box. The comparison of the background level in data with the predicted one can potentially improve the precision of the background estimate.

5.3 B Background Studies

We studied the main sources of B background in an earlier MC dataset generated for a collision energy of 10 TeV (Summer'09). We do not expect that the mixture of the different sources changes dramatically for a lower collision energy of 7 TeV. We list sources that contribute at least one event with a preliminary estimate of their contribution in the present sample. The final estimate of the contribution for a given integrated luminosity still needs to be performed on a consistently generated cocktail sample for 7 TeV.

The main categories are:

- $B_d \to J/\psi K^*$: the signature of this channel is very similar to the signal $B_s \to J/\psi\phi$ by replacing a kaon with a pion. This is the most important source of background and the selection has been done to optimize the discrimination between this channel and our signal.
- $B_d \to J/\psi K_1^0$: one of the feeddown channel for $B_s \to J/\psi\phi$. The K_1^0 meson primarily decays into ρ and a charged K. The misreconstruction occurs when the two charged pions from the ρ meson are, the first, identified as a charged K, the latter, lost.
- $B_d \to J/\psi K_S^0$: decay channel with K_s^0 decaying into two charged pions. The misreconstruction occurs where both charged pions are misidentified as charged kaons.
- $B_s \to J/\psi\eta$: one of the main background coming from B_s mesons. The knowledge of only the upper limit for the branching fraction make us overestimate this background channel.
- $B^+ \to J/\psi K^+$: one of the feedup channel for $B_s \to J/\psi\phi$. The charged K is matched to a flying K from the background to make a ϕ meson.
- Other B_s: all the decay of the B_s with daughter a J/ψ and any other particle
- Other B_d: all the decay of the B_d with daughter a J/ψ and any other particle
- Other: all the remaining decays from the hadronization of $b\bar{b}$ quarks

Table 6 lists potential background from other B_s decays, Table 7 from B_d decays, and Table 8 from B^+ decays.

B_s background		
Decay channel	# Ev.	BF
$J/\psi\eta$	8	$< 3.8 \times 10^{-3}$
$J/\psi\eta'$	2	$< 3.8 \times 10^{-3*}$
$D_s^{*+}e\bar{\nu_e}$	2	$(7.9 \pm 2.4)\%$
$D_s^{*+}\mu^+\nu_\mu$	2	$(7.9 \pm 2.4)\%$
$D_s^{*+}D_s^-$		$< 12.1\%$
$D_s^{*+}D_s^{*-}$		$< 25.7\%$
$D_{s1}^{'-}\mu^+\nu_\mu$		$(2.3 \pm 0.7) \times 10^{-3}$
$J/\psi(2S)K^+K^-$		$(6.8 \pm 3.0) \times 10^{-4}$
$D_s^{*+}D^0K^{*-}$		
$D^*(2010)^-\Delta^0\Sigma^-$		
$D_s^+D^-K^0$		
$\chi_{c1}(1P)\eta'$		
$K^0\pi^+D^*(2010)^-$		
$a_1^+D_s^-$		
$D_s^-\eta\rho^+$		
$\chi_{c1}\phi$		
$D_s^-\pi^0\pi^+$		
$D_s^{*-}\rho^+\rho^0$		
$K^*\pi^0D^{*0}$		
$D_s^{*-}\eta\rho^+$		
# of events	30	
# of events with ≥ 4 daughters	9	
Total	39	

Table 6: *Potential B_s background channels*

B_d background		
Decay channel	# Ev.	BF
$J/\psi K_1^0$	34	$(1.3 \pm 0.5) \times 10^{-3}$
$\rightarrow K\rho$	22	
$\rightarrow K^*(892)\pi$	5	
$\rightarrow K^+\pi^-\pi^0$	4	
$\rightarrow K^0\pi^+\pi^-$	3	
$J/\psi K^0$	5	$(8.71 \pm 0.32) \times 10^{-4}$
$D^*(2010)^- e^+ \nu_e$	3	$(5.16 \pm 0.11)\%$
$\chi_{c1} K^{*0}$	3	$(2.0 \pm 0.3) \times 10^{-4}$
$J/\psi K^+\pi^-$	3	$(1.2 \pm 0.6) \times 10^{-3}$
$J/\psi(2S) K^+\pi^-$	2	$< 1 \times 10^{-3}$
$J/\psi K_2^{*0}$	2	
$D^+ D^*(2010)^- K^0$	2	$(6.5 \pm 1.6) \times 10^{-3}$
$D^*(2010)^+ D_s^{*-}$		$(1.78 \pm 0.14)\%$
$D^*(2010)^+ \rho^0 \rho^-$		$(1.76 \pm 0.27)\%$
$D^*(2010)^- \eta\pi^+$		$(1.76 \pm 0.27)\%$
$J/\psi\rho^0$		$(2.7 \pm 0.4) \times 10^{-5}$
$\chi_{c1} K^-\pi^+$		$(3.8 \pm 0.4) \times 10^{-4}$
$D^*(2010)^+ D^*(2007)^0 K^-$		$(1.18 \pm 0.20)\%$
$D^*(2010)^- \omega\pi^+$		$(2.89 \pm 0.30) \times 10^{-3}$
$D^*(2010)^- D_s^{*+}$		$(8.2 \pm 1.1) \times 10^{-3}$
$D^*(2007)^0 \pi^+ K^-$		$< 6.9 \times 10^{-5}$
$D^*(2007)^0 D^0 K^0$		$< 6.6 \times 10^{-3}$
$D^*(2007)^0 \pi^+\pi^-$		$(6.2 \pm 2.2) \times 10^{-4}$
$J/\psi K^{*0}\pi^0$		$(6.6 \pm 2.2) \times 10^{-4}$
$D_s^{*+} D^-$		$(7.5 \pm 1.6) \times 10^{-3}$
$D^*(2010)^+ \omega\pi^-$		$(2.89 \pm 0.30) \times 10^{-3}$
$\chi_{c2} K^-\pi^+$		$< 3.6 \times 10^{-5}$
$D^*(2007)^0 D^- K^+$		$(4.6 \pm 1.0) \times 10^{-3}$
$J/\psi\omega$		$< 2.7 \times 10^{-4}$
$D_0^{*-} \tau \bar{\nu_\tau}$		
$D_1^+ e \bar{\nu_e}$		
$D^+ e^- \bar{\nu_e}$		
$D_1(2420)^- D_s^{*+}$		
$D^*(2010)^- \mu^+ \nu_\mu$		
$D^*(2010)^- K^+ K^{*0}$		
$D^+ \rho^0 \pi^-$		
$D^- \pi^+ \pi^0$		
$D_2^*(2460)^+ \tau \bar{\nu_\tau}$		
$D^*(2007)^0 \Sigma^{*0} \Sigma^{*0}$		
$\chi_{c1} K^0 \pi^0$		
$D^*(2010)^+ a_1^-$		
$D^*(2010)^+ \tau \bar{\nu_\tau}$		
$D_1^{'*-} \mu^+ \nu_\mu$		
$\eta' K^+ D_s^-$		
$D_1(2420)^+ \mu^+ \nu_\mu$		
$D^*(2010)^+ \rho^+ \eta$		
# of events	88	
# of events with ≥ 4 daughters	22	
Total	110	

Table 7: *Potential B_d bacjground channels.*

Other background		
Decay channel	# Ev.	BF
$B^+ \to J/\psi K_1^+$	17	$(1.8 \pm 0.5) \times 10^{-3}$
$B^+ \to J/\psi K^{*+}$	4	$(1.43 \pm 0.08) \times 10^{-3}$
$B^+ \to J/\psi K^+$	4	$(1.007 \pm 0.035) \times 10^{-3}$
$B^+ \to D^*(2007)^0 \tau^+ \nu_\tau$	3	$(2.2 \pm 0.6)\%$
$B^- \to D^0 e \bar{\nu_e}$	2	$(2.24 \pm 0.11)\%$
$B^+ \to D^*(2007)^0 e^+ \nu_e$	2	$(5.68 \pm 0.19)\%$
$B^+ \to D^*(2007)^0 \mu^+ \nu_\mu$	2	$(5.68 \pm 0.19)\%$
$B^- \to J/\psi(2S) K^-$	2	$(6.48 \pm 0.35) \times 10^{-4}$
$B^- \to \chi_{c1} K^{*-}$	2	$(3.6 \pm 0.9) \times 10^{-4}$
$B^+ \to \chi_{c1} K^+$		$(5.1 \pm 0.5) \times 10^{-4}$
$B^+ \to D_s^{*+} D^0$		$(7.8 \pm 1.6) \times 10^{-3}$
$B^+ \to J/\psi pi^+$		$(4.9 \pm 0.6) \times 10^{-5}$
$B^- \to D^*(2007)^0 D^*(2010)^- K^0$		$(7.8 \pm 2.6) \times 10^{-3}$
$B^- \to D^*(2007)^0 D^*(2007)^0 K^-$		$(5.3 \pm 1.6) \times 10^{-3}$
$B^+ \to D_0^{*0} e^+ \nu_e$		$(2.5 \pm 0.5) \times 10^{-3}$
$B^- \to D_s^{*+} D^*(2007)^0$		$(1.74 \pm 0.23)\%$
$B^- \to D_s^{*-} D^+ \pi^-$		
$B^+ \to J/\psi K_1^{'+}$		
$B^+ \to D_2^*(2460)^0 D_s^+$		
$\Lambda_b \to J/\psi(2S)\Lambda$		
$B^+ \to D^*(2007)^0 D_{s1}(H)^+$		
$\Lambda_b \to J/\psi\Lambda$		
$B^+ \to D_s^+ D^0 \pi^0$		
$B^+ \to \rho^0 \Sigma_c^- \Delta^{++}$		
$\Lambda_b \to \Lambda_c^+ D_s^{*-}$		
$B^- \to J/\psi D_{s0}^{*-}$		
# of events	55	
# of events with ≥ 4 daughters	10	
Total	65	

Table 8: *Potential background B^+ decay channels.*

5.4 Systematic Error

For the cut-and-count analysis we establish the following efficiencies and potential biases (corrections):

- trigger
- charged particle tracking
- B vertexing (production vertex)
- muon reconstruction, J/ψ candidate reconstruction

and estimate systematic uncertainties for those. Furthermore, we consider ...

6 Maximum Likelihood (ML) fit

We extract signal yields and lifetimes from the selected samples using an unbinned extended maximum-likelihood fit to the mass M_{B_s} and proper decay length ct of the reconstructed candidates.

6.1 Selection

We change some requirements with respect to our cut-and-count analysis in Sec. 5 on the event variables: we remove the requirement on $\cos\alpha$ and the lifetime significance $ct/\sigma(ct)$ since they present a bias to ct. Furthermore, we tighten the requirement on the invariant K^+K^- mass to lie within 10 MeV of the world average value and the B_s invariant mass between 5.25 and 5.65 GeV/c^2. This allows us to strongly suppress background events from $B_d \to J/\psi K^*$ that have been misreconstructed. The total selection efficiency is $\epsilon = 28.3\%$. The expected composition of the final sample for the fit for an integrated luminosity of 1 pb^{-1} as derived from simulated event samples is listed in Table 9.

	$B_s \to J/\psi\phi$	$b \to X$	Prompt J/ψ	$pp \to \mu\mu X$
Number of generated events	970	94736	920247	510216
`L1DoubleMuOpen`	191	17514	98854	210566
Pre Kinem. fit	121	10266	39362	6597
After Kinem. fit	84	1653	3408	1432
Vtx P(KK)>2 %	76	1008	2406	548
Kaon $p_T > 0.7$ GeV/c	64	397	857	243
$\Delta\phi$ mass < 10 MeV	54	98	213	57

Table 9: *Sample composition in 1 pb^{-1} for the Maximum Likelihood fit as predicted from studies of simulated events.*

The event distribution in the two variables M_{B_s} and ct for the different samples is presented in Fig. 20 and Fig. 21, respectively.

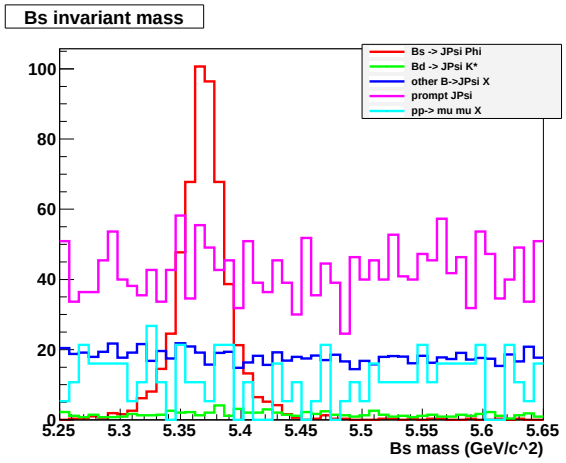

Figure 20: B_s invariant mass distribution after the "ML" selection for the signal and background categories.

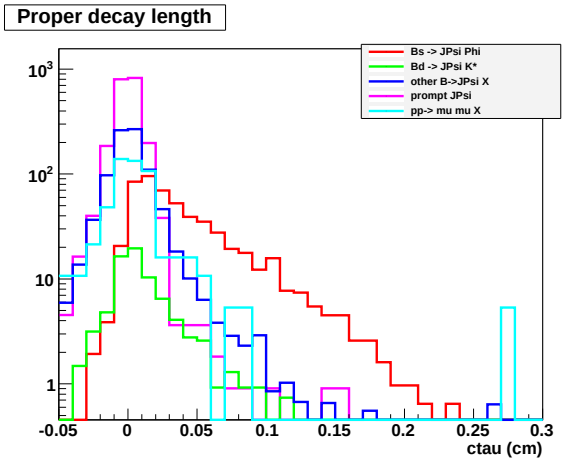

Figure 21: B_s proper decay length distribution after the "ML" selection for the signal and background categories.

6.2 Preparation

Since we measure the correlations among the observables to be small in the samples entering the fit, we take the probability density function $\mathcal{P}^j_{i,c}$ for each event j to be a product of the PDFs for the separate observables. For each event hypothesis i (signal, backgrounds), we define

$$\mathcal{P}^j_i = \mathcal{P}_i(M_{B_s};\alpha_i)\cdot\mathcal{P}_i(ct,\sigma_{ct};\beta_i)\,, \tag{6}$$

with shape parameters α_i for M_B and β_i for ct, evaluated separately for each of the components i. The σ_{ct} is the error on ct for a given event. We consider three separate components (i): signal, B background and prompt J/ψ.

The extended likelihood function for the sample is given as:

$$\mathcal{L} = \exp\left(-\sum_i n_i\right) \prod_j \left[\sum_i n_i P_i^j\right] \tag{7}$$

The yields n_i and lifetime τ_i for each sample are then determined by minimizing the quantity $-\ln \mathcal{L}$ [**?**].

The analysis proceeds with the fit of the entire sample floating yields and the B proper decay length from which we can extract the lifetime. The PDFs are constructed from common functions (Gaussian, exponential, etc) and the parameters are determined on the available data samples. The guiding principle we follow in designing the PDFs is to use the simplest function with the least number of parameters necessary to adequately describe the observed distribution of events for M_B and ct for each component. For the signal $B_s \rightarrow J/\psi\phi$, we tried to parameterize the B_s invariant mass with two and three Gaussian distributions (Fig. 22 and Fig. 23) but we choose the three-Gaussians parameterization. For the proper decay lenght ct, generated with value $c\tau = 424$ ps, we fit an exponential convoluted with a gaussian with and without error correction event by event (Fig. 24 and Fig. 25). For the final fit we will use the PDF with error correction event by event. In Table 10 the summary of the PDFs used for each component.

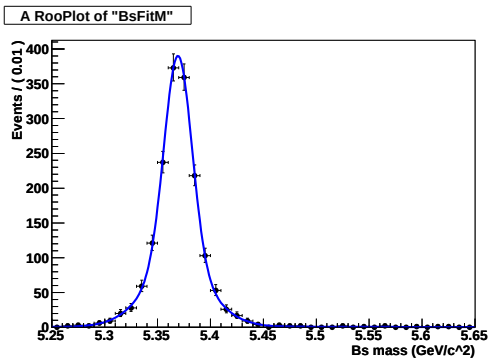

Figure 22: B_s invariant mass signal distribution fitted with three Gaussians.

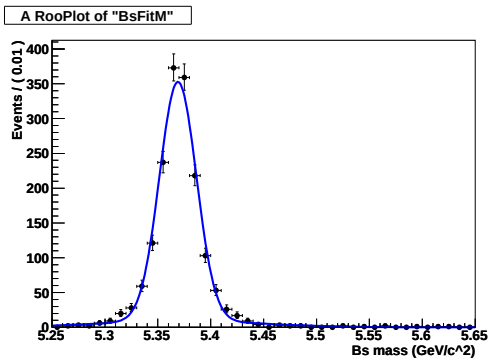

Figure 23: B_s invariant mass signal distribution fitted with two Gaussians.

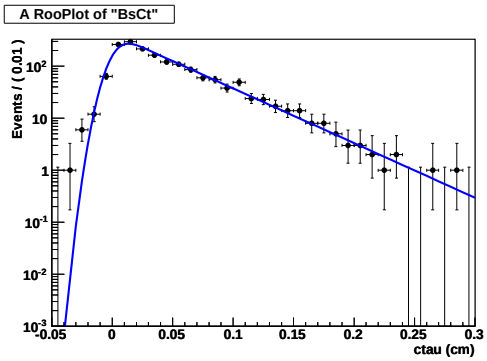

Figure 24: B_s proper decay length signal distribution without event by event correction.

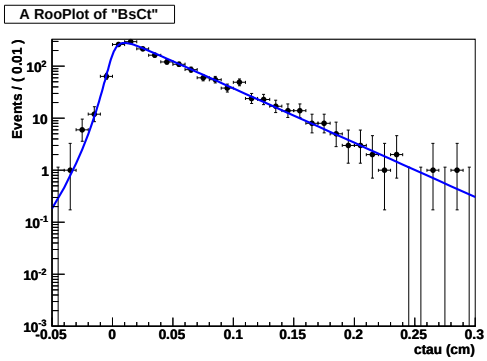

Figure 25: B_s proper decay length signal distribution with event by event correction.

For the B cocktail background we parameterize the B_s invariant mass with a first degree Chebychev polynomial while a double Gaussian convoluted with a double-sided exponential for the proper decay length.

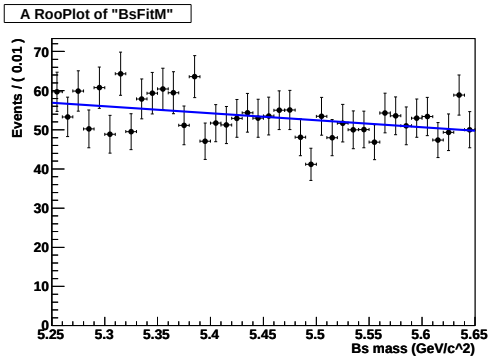

Figure 26: B_s invariant mass for B background distribution.

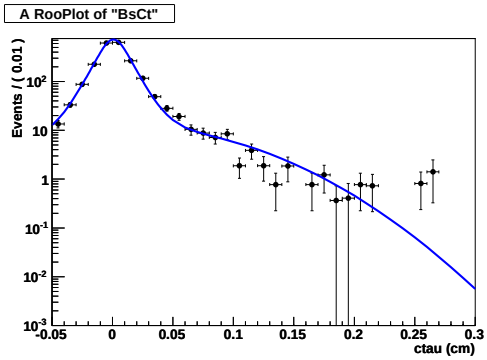

Figure 27: B_s proper decay length for B background distribution.

For the prompt J/ψ background we parameterize the B_s invariant mass with a first degree Chebychev polynomial while a double Gaussian convoluted with a double-sided exponential for the proper decay length.

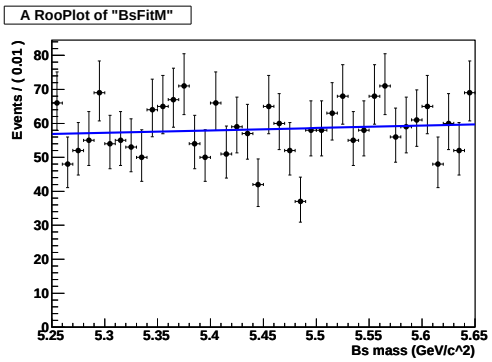

Figure 28: B_s invariant mass for prompt background distribution.

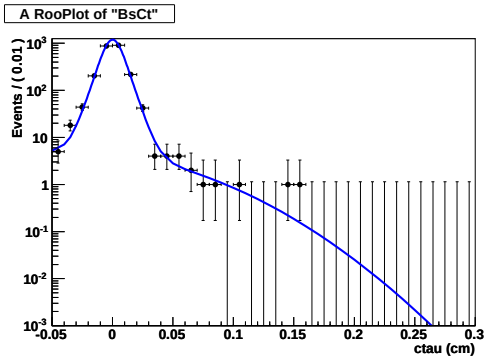

Figure 29: B_s proper decay length for prompt background distribution.

	M_B		ct	
Components	Function	Parameters	Function	Parameters
Signal	$G_1 + G_2 + G_3$	$\{\mu_i, \sigma_i\}$	$G_1 \otimes e^{-ct/\lambda}$	$\{\mu_i, \sigma_i, \lambda\}$
B background	Pol1	$\{\alpha\}$	$(G_1 + G_2) \otimes e^{\mp ct_\pm/\lambda_\pm}$	$\{\mu_i, \sigma_i, \lambda_\pm\}$
Prompt J/ψ	Pol1	$\{\alpha\}$	$(G_1 + G_2) \otimes e^{\mp ct_\pm/\lambda_\pm}$	$\{\mu_i, \sigma_i, \lambda_\pm\}$

Table 10: Summary of M_B and ct PFDs used in the fit. Where more than one Gaussian (G) is used in a function we denote the separate means and widths with the notation μ_i and σ_i, where i is an index that runs over the number of Gaussians (either two or three). For B background and prompt J/ψ we describe the long tails in the resolution function with two separate exponential functions, one for $ct > 0$ and the other for $ct < 0$.

6.3 Fit Validation

We have performed a series of detailed studies to demonstrate the accuracy and robustness of our fit strategy. To prove that the fit configuration is unbiased, we have done 100 toy experiments generating the number of expected signal and background yields according to an integrated luminosity of 3 pb^{-1} For each category we examined fitted value for the yields with their errors and the possible bias ("pull" distributions). We confirm that no biases are observed, and the errors are properly estimated from the fit (see. Table 8).

Components	Generated yield	Fitted yield	Pull mean	Pull sigma
Signal	161	164 ± 16	0.13 ± 0.09	0.937 ± 0.066
B background	291	296 ± 64	0.09 ± 0.10	1.022 ± 0.072
Prompt J/ψ	636	634 ± 64	-0.19 ± 0.11	1.130 ± 0.080

Table 11: Summary table of 100 toy experiments with yields generated from the PDFs.

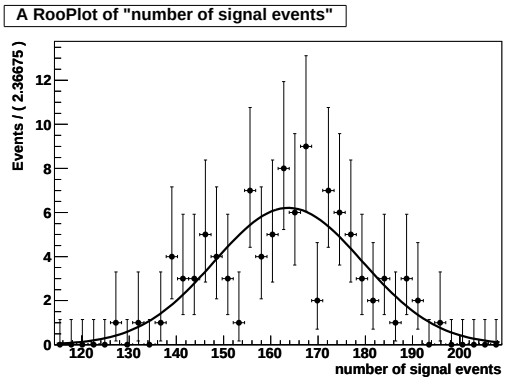

Figure 30: Signal yield distribution.

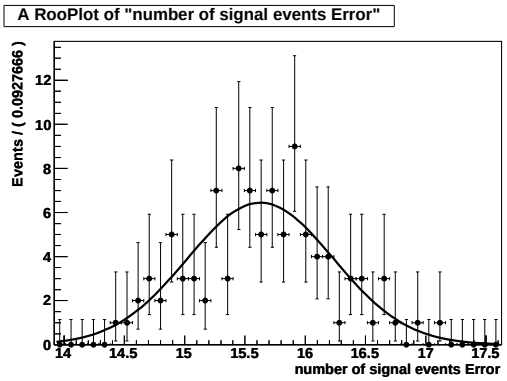

Figure 31: Signal yield error distribution.

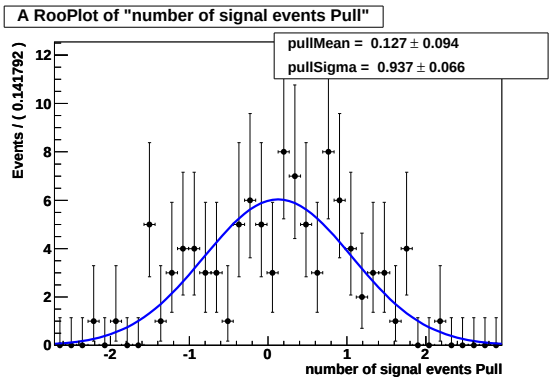

Figure 32: Signal yield distribution.

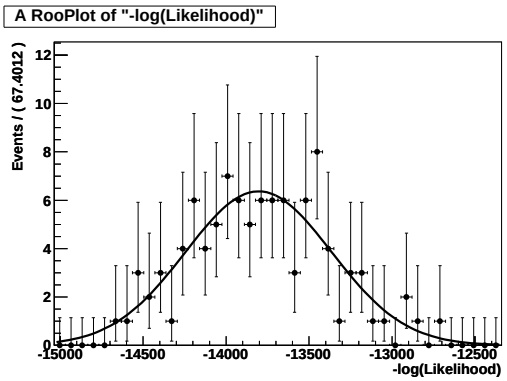

Figure 33: Negative logarithmic likelihood distribution.

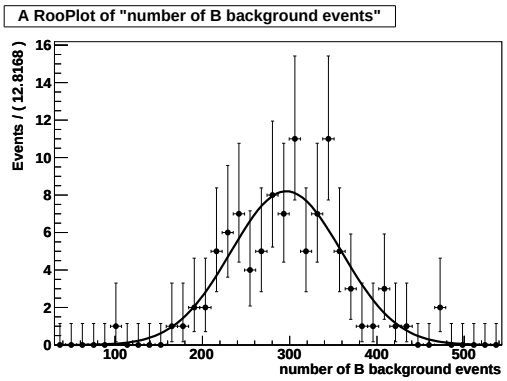

Figure 34: B background yield distribution.

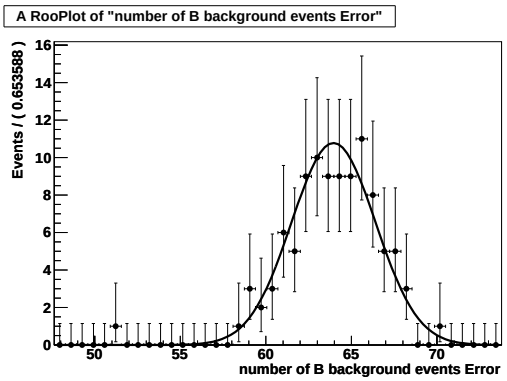

Figure 35: B background yield error distribution.

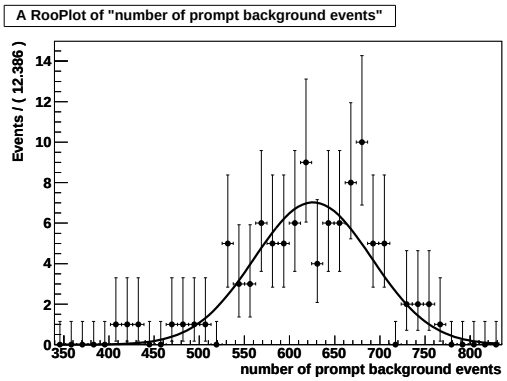

Figure 36: Prompt background yield distribution.

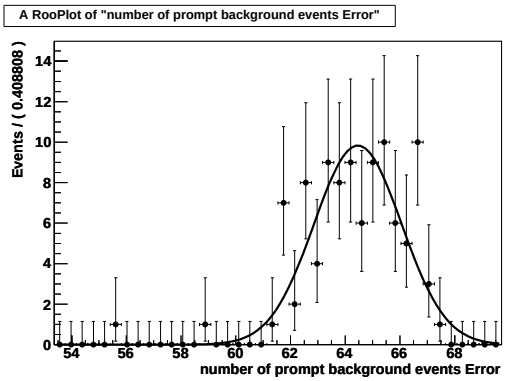

Figure 37: Prompt background yield error distribution.

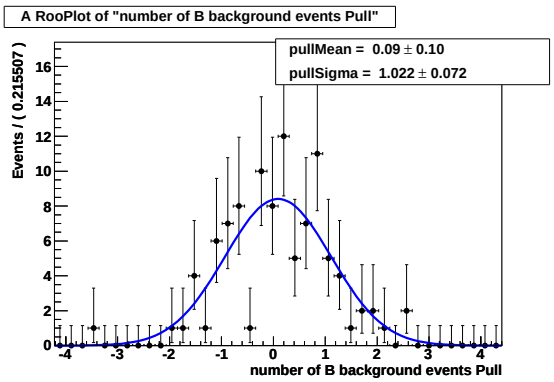

Figure 38: B background pull distribution.

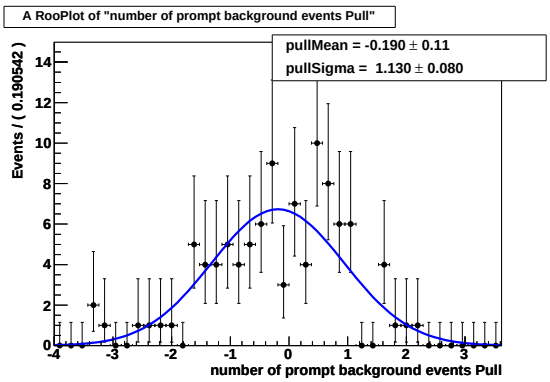

Figure 39: Prompt background pull distribution.

We repeat the experiment fitting 100 independent MC cocktail samples with the number of expected events for each category. In the fit we let free to float the yields, the proper decay length for $B_s \rightarrow J/\psi\phi$, the bias and the scaling factor of the signal resolution function. This test has been performed with statistics for three different integrated luminosity (3 pb^{-1}, 1 pb^{-1} and 0.5 pb^{-1}).

Components	Expected	Fit value
Signal	161	189 ± 19
B background	291	245 ± 63
Prompt J/ψ	636	639 ± 62
λ (μm)	424	425 ± 38
Bias		-1.48 ± 0.35
Scaling factor		1.08 ± 0.28

Table 12: Summary table for experiments with integrated luminosity of 3 pb^{-1}.

Components	Expected	Fit value
Signal	54	65 ± 11
B background	97	82 ± 36
Prompt J/ψ	212	215 ± 35
λ (μm)	424	429 ± 56
Bias		-1.53 ± 0.64
Scaling factor		1.25 ± 0.46

Table 13: Summary table for experiments with integrated luminosity of 1 pb^{-1}.

Components	Expected	Fit value
Signal	27	34 ± 7
B background	49	42 ± 26
Prompt J/ψ	106	110 ± 25
λ (μm)	424	401 ± 80
Bias		-1.65 ± 1.18
Scaling factor		1.72 ± 0.81

Table 14: Summary table for experiments with integrated luminosity of 0.5 pb^{-1}.

It is generally expected that the real backgrounds encountered in collision data could be much higher than predicted by the default (untuned) CMS full simulation samples.

6.4 Fit results

As previously mentioned, we first perform a fit to determine lifetimes and total yields. In Fig. 40 and Fig. 41 the fitted distributions of M_B and $c\tau$ for the B_s sample are shown assuming an integrated luminosity of 3 pb^{-1}. The plots show the total contribution from signal and background components (solid blue line) and the different components. Table 12 summarizes the fitted yields and lifetime for the sample considered.

Components	$B_s \to J/\psi\phi$
Signal	179 ± 17
λ (μm)	424 ± 41
Generated λ (μm)	424
B background	244 ± 63
Prompt J/ψ	664 ± 64
Bias	-1.29 ± 0.43
Scaling factor	1.06 ± 0.44

Table 15: Summary of the ML fit on the MC dataset.

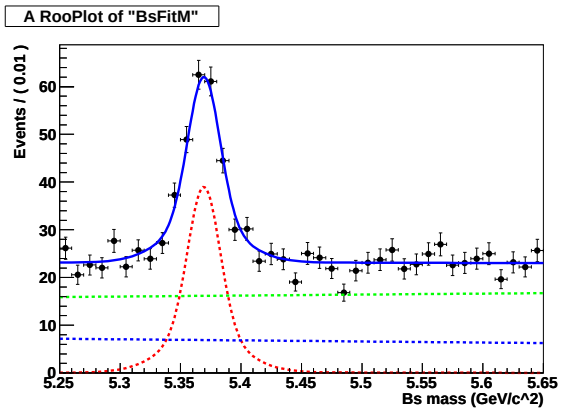

Figure 40: Projection of the fit onto the B_s invariant mass variable (solid blue) with the different components: signal (dashed red), B background (dashed blue) and prompt J/ψ background (dashed green).

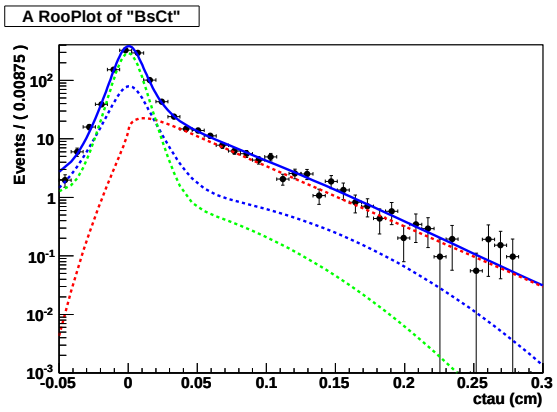

Figure 41: Projection of the fit onto the B_s proper decay length variable (solid blue) with the different components: signal (dashed red), B background (dashed blue) and prompt J/ψ background (dashed green).

7 Systematics

We have considered several sources of systematic uncertainty on the lifetime measurement. The different contributions are:

- To be done.

References

[1] I. Dunietz, R. Fleischer, and U. Nierste, "In persuit of new physics with B_s decays", Phys. Rev. **D63** (2001) 114015.

[2] A.S. Dighe, I. Dinietz, and R. Fleischer, "Extracting CKM phases and B_s-$\bar{B}_s$ mixing parameters from angular distributions of non-leptonic B decays", Eur. Phys. J. **C6** (1999) 647; A.S. Dighe, I. Dunietz, H.J. Lipkin, and J.L. Rosner, "Angular distributions and lifetime differences in $B_s \to J/\psi\phi$ decays", Phys. Lett. **B369** (1996) 144.

[3] C. Amsler et al. (Particle Data Group), Phys. Lett. **B667** (2008) 1.

[4] Lotte Wilke, "Study of the B_s-Meson with the First LHC Data", Ph.D. University of Zuerich (2009).

[5] P. Nason et al., "Bottom production", Proceedings of the Workshop on Standard Model Physics (and more) at the LHC, CERN, 2000.

[6] J.M. Campbell, J.W. Huston, W.J. Stirling, "Hard Interactions of Quarks and Gluons: A Primer for LHC Physics", Rep. Prog. Phys **70** (2007) 89.

[7] J. Baines et al., "Heavy Quarks (Working Group 3): Summary Report for the HERA-LHC Workshop Proceedings", arXiv:hep-ph/0601164.

[8] J.R. Klein, A. Roodman, "Blind Analysis in Nuclear and Particle Physics", Annu. Rev. Nucl. Part. Sci. 55 (2005) 141.

[9] CMSSW

[10] H.-U. Bengtsson and T. Sjostrand, "The Lund Monte Carlo for Hadronic Processes: Pythia Version 4.8", Comput. Phys. Commun. **46** (1987) 43.

[11] EvtGen

[12] Presentation at the Trigger Meeting, March, 2010. We update the study as new scenarios are defined.